

Shear Induced Formation of Patterned Porous Titania with Applications to Photocatalysis

Xiangcun Li,^{†,‡} Vijay T. John,^{*,†} Gaohong He,[‡] Jingjing Zhan,[†] Grace Tan,[†] Gary McPherson,[†] Arijit Bose,[§] and Jayashri Sarkar[§]

[†]Department of Chemical and Biomolecular Engineering, Tulane University, New Orleans, Louisiana 70118,

[‡]State Key Laboratory of Fine Chemicals, The R&D Center of Membrane Science and Technology, Dalian University of Technology, Dalian 116012, China, and [§]Department of Chemical Engineering, University of Rhode Island, Kingston, Rhode Island 02881

Received January 14, 2009. Revised Manuscript Received April 21, 2009

Patterned macroporous titania (TiO_2) materials have been synthesized via a shear-aligned rigid crystalline surfactant mesophase. The macropores inherit the hexagonal geometry of the water channels of the template. Scanning electron microscopy (SEM) and cut-section transmission electron microscopy (TEM) images show that the macropores templated by the sheared mesophase attain considerably greater alignment than pores templated by the nonsheared mesophase. The mean pore diameter, the crystalline size of TiO_2 particles, and the photoactivity of the materials increase with the increase of water content in the template. The sheared TiO_2 samples exhibit higher photocatalytic activity for the degradation of Rhodamine B than the corresponding materials synthesized in the nonsheared template. The improvement in photocatalytic activity of the sheared TiO_2 materials is attributed to its higher photoabsorption efficiency and the patterned channels which facilitate the diffusion and transport of reactant molecules within the frameworks. Such patterned porous materials may have promise as advanced catalytic supports and photocatalytic materials.

Introduction

Titania (TiO_2) has been extensively studied as an effective photocatalyst for the photooxidation of various organic pollutants present in wastewater and air,^{1,2} with applications in drinking water treatment and disinfection.³ Increasing attention has been focused on the preparation of titania materials with organized mesopores/macropores (IUPAC nomenclature defines pores between 2 and 50 nm as mesopores and pores greater than 50 nm as macropores). Such materials may provide interesting potential applications in photocatalysis. The pores can act as light transfer paths to introduce an increased amount of photo energy onto the inner surface of TiO_2 . With organized pores, it is possible for a significant number of photoactive sites to be activated by light reflection and scattering, thereby improving the light harvesting and the photoabsorption efficiency of the catalyst. Additionally, patterned large channels may facilitate diffusion of reactant molecules within the porous framework and enhance the reaction rate. For example, macroporous TiO_2 materials with 1–2 μm channels arranged parallel to each other exhibit higher efficiency for photooxidation of ethylene than Degussa P-25 titania because the macrochannels increase photoabsorption

efficiency and allow easy diffusion of gaseous molecules.^{1b} Highly patterned mesoporous carbon–titania nanocomposites show excellent photocatalytic performance for the degradation of Rhodamine B in an aqueous suspension, which can be attributed to the high adsorption capacity from the large surface area and the ordered ~4.1 nm mesopores.⁴ For the synthesis of patterned mesoporous/macroporous arrays of titania materials, a variety of techniques have been devised, such as the micelle-templated method,^{1b} in situ crystallization technology,⁴ replication of citric-acid-templated mesoporous silica,⁵ chemical etching through anodic alumina membranes into TiO_2 ,⁶ and ion beam lithography through a porous alumina mask.⁷ However, these sequential approaches entail disadvantages such as complex synthesis procedures and expensive microfabrication instrumentation.

In this paper, we describe a new self-assembly based method to synthesize porous titania with patterned channels and applications to photocatalysis, using surfactant based templates. The use of self-assembly to direct materials synthesis is an area of tremendous interest.⁸ However, achieving high fidelity between the actual ceramic morphology and surfactant template microstructures remains a significant challenge in materials synthesis in self-assembled soft templates.⁹ While porous solids are easily obtained, there often is little relation between the ceramic

*Corresponding author. E-mail: vj@tulane.edu. Telephone: (504) 865-5883. Fax: (504) 865-6744.

(1) (a) Song, X. F.; Gao, L. *J. Phys. Chem. C* **2007**, *111*, 8180. (b) Wang, X. C.; Yu, J. C.; Ho, C.; Hou, Y. D.; Fu, X. Z. *Langmuir* **2005**, *21*, 2552. (c) Srinivasan, M.; White, T. *Sci. Technol.* **2007**, *41*, 4405. (d) Tran, T. H.; Nosaka, A. Y. *J. Phys. Chem. B* **2006**, *110*, 25525.

(2) (a) Jiang, X.; Wang, T. *Environ. Sci. Technol.* **2007**, *41*, 4441. (b) Ren, M.; Ravikrishna, N. R.; Valsaraj, K. T. *Environ. Sci. Technol.* **2006**, *40*, 7029. (c) Xie, C.; Yang, Q. J.; Xu, Z. L.; Liu, X. J.; Du, Y. G. *J. Phys. Chem. B* **2006**, *110*, 8587. (d) Inaba, R.; Fukahori, T.; Hamamoto, M.; Ohno, T. *J. Mol. Catal. A: Chem.* **2006**, *260*, 247.

(3) (a) Wu, J. M.; Zhang, T. W.; Zeng, Y. W.; Hayakawa, S.; Tsuru, K.; Osaka, A. *Langmuir* **2005**, *21*, 6995. (b) Pelizzetti, E.; Minero, C.; Borgarello, E.; Tinucci, L.; Serpone, N. *Langmuir* **1993**, *9*, 2995. (c) Yu, J. C.; Ho, W.; Yu, J. G.; Yip, H.; Wong, P. K.; Zhao, J. C. *Environ. Sci. Technol.* **2005**, *39*, 1175. (d) Zhao, W.; Sun, Y. I.; Castellano, F. N. *J. Am. Chem. Soc.* **2008**, *130*, 12566.

(4) Liu, R. L.; Ren, Y. J.; Shi, Y. F.; Zhang, F. L.; Zhang, J.; Tu, B.; Zhao, D. Y. *Chem. Mater.* **2008**, *20*, 1140.

(5) Lee, D. W.; Park, S. J.; Ihm, S. K.; Lee, K. H. *Chem. Mater.* **2007**, *19*, 937.

(6) Hideki, M.; Kazuyuki, N.; Nobuyoshi, B. *Jpn. J. Appl. Phys.* **1992**, *31*, 1775.

(7) Sanz, R.; Johansson, A.; Skupinski, M.; Jensen, J.; Possnert, G.; Boman, M.; Vazquez, M.; Hjort, K. *Nano. Lett.* **2006**, *6*, 1065.

(8) (a) Stathatos, E.; Lianos, P.; Monte, F. D.; Levy, D.; Tsiorvas, D. *Langmuir* **1997**, *13*, 4295. (b) Stathatos, E.; Lianos, P.; Falaras, P.; Siokou, A. *Langmuir* **2000**, *16*, 2398. (c) Choi, H.; Kim, Y. J.; Varma, R. S.; Dionysiou, D. D. *Chem. Mater.* **2006**, *18*, 5377. (d) Caruso, R. A.; Giersig, M.; Willig, F.; Antonietti, M. *Langmuir* **1998**, *14*, 6333. (e) Caruso, R. A.; Susha, A.; Caruso, F. *Chem. Mater.* **2001**, *13*, 400.

(9) Pileni, M. P. *Nat. Mater.* **2003**, *2*, 145.

structure and the original organic gel microstructure. Thermal fluctuations in liquid systems where small amphiphile self-assembly results from relatively weak noncovalent interactions may be a simple explanation why template fidelity is lost in the final ceramic structure. For example, in the case of the MCM-41S materials,¹⁰ the soft templates change structure or break down with incorporation of additional chemical species and it is not immediately evident that micelles get templated into mesoporous materials. While there is little relationship between the structure of the mesoporous MCM-41 material and the structure of an individual micelle, a rational explanation is that collisions between micelles leads to the linkages between silica growing on separate micelles and further self-assembly resulting in the formation of structured mesoporous ceramics.

We show here a sufficiently rigid crystalline surfactant mesophase that can be shear-aligned to create templates for materials synthesis, and that the structure of the template is reflected in the morphology of the ceramic. The system that is used contains the anionic surfactant AOT (2-ethylhexyl sodium sulfosuccinate) mixed with the zwitterionic phospholipid lecithin (α -phosphatidylcholine), in the molar ratio of 2:1. When this two-surfactant mixture is dissolved in a nonpolar solvent (e.g., isoctane) and water is progressively added, the system evolves from a low viscosity solution to a gel-like state with crystalline order illustrated through small angle neutron scattering measurements.¹¹ For example, over the composition range surfactant/isoctane/water 0.27/0.27/0.46 to 0.21/0.21/0.57 (in weight fractions), the surfactant mesophase has columnar hexagonal symmetry, with water cylindrical columns arranged in hexagonal geometry (the H_{II} phase). The system is optically clear, has a high viscosity up to 10^6 Pa·s at low shear rates, and has a relatively high rigidity as characterized by a storage modulus (G') of 10^4 Pa.¹²

The following characteristics encouraged us to conduct materials synthesis in these systems. (1) Significant shear alignment is obtained with relatively low shear rates, typically less than 10 s^{-1} . (2) In such a relatively rigid system, once shear has been employed, the alignment persists for extended periods approaching a week.¹³ Figure 1a reproduced from our earlier work on this system illustrates small angle neutron scattering patterns for the surfactant mesophase where D_2O has been used instead of water to provide sufficient contrast. It shows scattering profiles obtained in a Couette cell, providing information in both the flow-vorticity (radial) and flow-gradient-vorticity (tangential) planes. The radial and tangential scattering profiles of the samples prior to application of shear show typical powder diffraction patterns, and no significant differences are observed. The scattering profiles at the bottom of Figure 1a illustrate the dramatic alignment of the system after it is fully subjected to shear. The convergence to a two-spot pattern in the radial profile and the six spot patterns in the tangential profile are characteristic of aligned columnar hexagonal structures.^{12,14} Figure 1b shows a scanning cryo-electron micrograph of the hexagonal structure of the soft template showing crystalline domains.¹⁵

(10) Beck, J. S.; Vartuli, J. C.; Roth, W. J.; Leonowicz, M. E.; Kresge, C. T.; Chu, W.; Olson, D. H.; Sheppard, E. W. *J. Am. Chem. Soc.* **1992**, *114*, 10834.

(11) Simmons, B. A.; Irvin, G. C.; Agarwal, V.; Bose, A.; John, V. T.; McPherson, G. L.; Balsara, N. P. *Langmuir* **2002**, *18*, 624.

(12) Singh, M.; Agarwal, V.; De Kee, D.; Bose, A.; McPherson, G.; John, V. T. *Langmuir* **2004**, *20*, 5693.

(13) Liu, L. M.; John, V. T.; McPherson, G. L.; Maskos, K.; Bose, A. *Langmuir* **2005**, *21*, 3795.

(14) Ramos, L. M.; Porte, G. F. *Langmuir* **2000**, *16*, 5846.

(15) Tan, G.; Xu, P.; He, J. B.; McPherson, G. L.; Agarwal, V.; Bose, A.; John, V. T. *Langmuir* **2008**, *24*, 10621.

In this paper, we exploit these ideas to form aligned titania structures based on shear alignment of the viscous surfactant soft template. Diameters of the channels can also be tuned by adjusting the water content without altering the qualitative features of the TiO_2 microstructure. In particular, we show that it is possible to generate hierarchically porous structures that contain mesopores ($< 50\text{ nm}$) together with larger macropores ($> 200\text{ nm}$). While the macropores may serve to enhance light transmission to the particle interior, the mesopores may increase residence times of diffusing species, thus enhancing photocatalytic degradation. In this work, Rhodamine B photodegradation was employed as a probe reaction to test the photoactivity of the titania samples.

Materials and Methods

Titanium isopropoxide (TIP), isoctane, and dioctyl succinate sodium salt (AOT) were purchased from Sigma Aldrich. Lecithin ($\text{L}-\alpha$ -phosphatidylcholine, Soy-95%) was obtained from Avanti Polar Lipids. Distilled water was used in all experiments.

Sample Preparation. TiO_2 samples were synthesized at room temperature in a bisurfactant system consisting of anionic surfactant (AOT)/zwitterionic lecithin with isoctane as solvent. When this surfactant mixture with 2:1 mol ratio is dissolved in a nonpolar solvent, for example, isoctane, and water is progressively added, the system evolves from a solution to a high viscosity gel with water cylindrical columns arranged in hexagonal geometry. In a typical synthesis of TiO_2 , TIP was added to the solution of isoctane/AOT(0.8 M)/lecithin(0.4 M), holding the volume ratio of TIP to isoctane at 1:1. A transparent yellow color microemulsion was obtained. A designated amount of water, corresponding to the W_0 values ($W_0 = [\text{water}]/[\text{AOT}]$, mole ratio), was progressively added to the AOT/lecithin/TIP mixture and mixed using a vortex mixer. The sample was dried at 60°C for 1 day and calcined by ramping the temperature 50°C every 30 min from 400 to 550°C in order to remove the surfactants and organic solvent. The sample was then left at 550°C for 5 h to obtain a white TiO_2 powder. For the preparation of titania products containing aligned channels, the sample containing water was transferred into a stainless steel tube immediately after vortex mixing, after which the tube was attached to the spindle of a Bohlin viscometer, and the sample was sheared at a rate of 24.0 s^{-1} for 60 min. When shearing was completed, the sample was allowed to dry at 60°C for 1 day in the tube. The calcination procedure was the same as that followed for the nonsheared samples.

Photocatalytic Experiments. The photocatalytic activity of each TiO_2 sample was evaluated by the degradation of Rhodamine B in deionized water. The reaction was carried out in a RPR-100 Rayonet reactor (1.65×10^{16} photons/s/cm³), operated at 35°C . The bulbs produced a strong peak centered at 254 nm. No additional filters were used, and the distance between the sample and the around bulbs was about 15 cm. In a typical process, 10 mg of TiO_2 was added to 50 mL of a $1.0 \times 10^{-5}\text{ mol L}^{-1}$ Rhodamine solution and magnetically stirred in the dark for 30 min prior to irradiation, to achieve adsorption equilibrium of Rhodamine B with the catalyst. The samples were collected every 20 min by centrifugation to determine the degradation rate by UV-vis adsorption (553.5 nm, Shimadzu UV 1700).

Characterization. Electron Microscopy. Scanning electron microscopy (SEM) was performed on a Hitachi-4800 field emission scanning microscope operated at 7 kV to investigate the channel morphology and microstructure. For cut-section transmission electron microscopy (cut-section TEM), the powder samples were embedded in an epoxy resin, dried overnight, and ultramicrotomed into thin slices (approximately 70 nm) with a diamond knife. A thin slice of the microtomed sample was transferred to a copper grid and viewed on a JEOL 2010 transmission electron microscope operated at 200 kV.

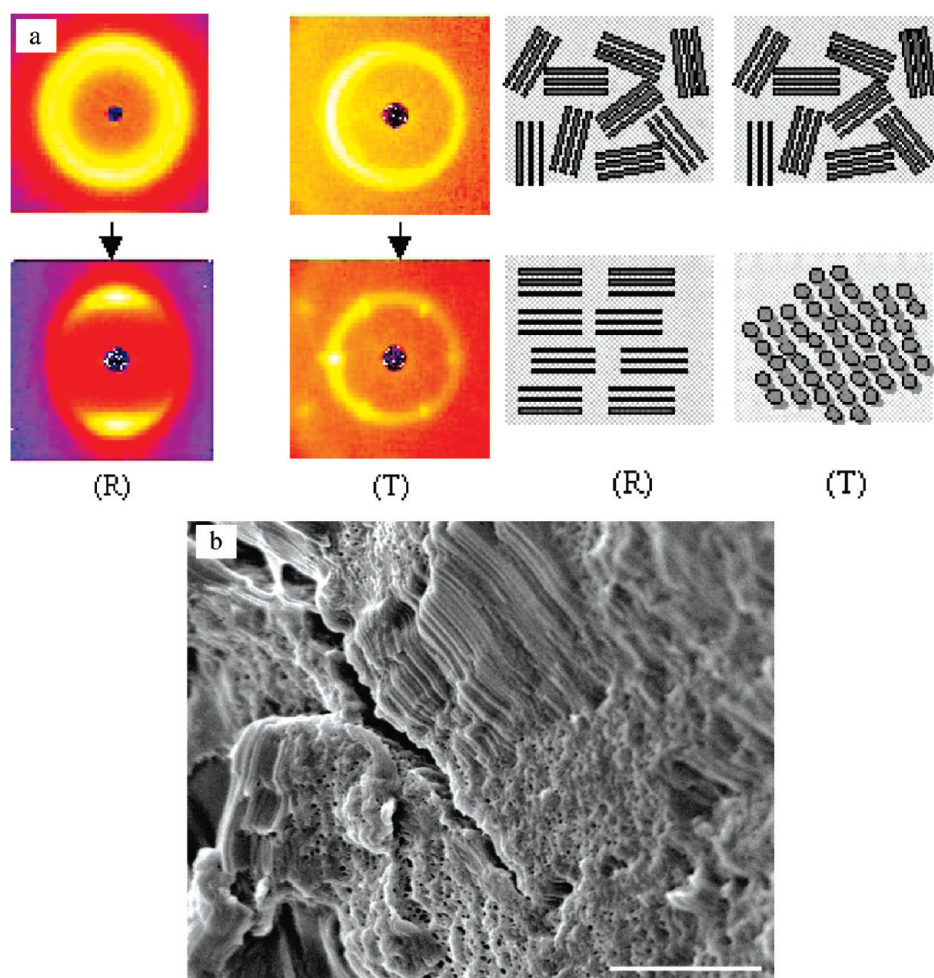


Figure 1. (a) Scattering profiles of the template in radial (R) and tangential (T) modes. At the top are the profiles prior to shear, and at the bottom are profiles after application of shear when alignment has set in. On the right are idealized representations of the alignment. (b) Cryo-scanning electron micrograph of the surfactant template showing the crystalline domains. The application of shear leads to long-range alignment of these domains. The scale bar is 1 μ m.

X-ray Diffraction (XRD) and Surface Area Measurements. The XRD patterns were recorded on a Scintag XDS 2000 powder diffractometer using Cu K α radiation of wavelength 1.54 Å in the range of 20–80° (2 θ) and a 2 θ scan rate of 2°/min. The accelerating voltage and the applied current were 43 kV and 38 mA, respectively. The average crystalline size was estimated by the Scherrer formula based on the full width at half maxima (fwhm) of the X-ray diffraction peak. Nitrogen adsorption–desorption isotherms at 77 K for mesoporous titania samples were obtained using the Micromeritics ASAP 2010 instrument. The specific surface area was calculated using the Barret–Joyner–Halender (BJH) method.

Results and Discussion

Typical SEM (a, c, e) and cut-section TEM (b, d, f) images of TiO₂ samples synthesized by the soft templates at $W_0 = 70, 100, 150$, respectively, are shown in Figure 2. We clearly observe that domains of the crystalline mesophase are templated into ceramic structures. At the surface of the particles, the channels are extremely narrow and reflect the dimensions of the soft template. We then see the channels opening up to larger channels. Thus, the TIP hydrolyzes at the oil–water interface to form the TiO₂ support wall, and the morphology of hexagonal water channels is preserved and inherited by the hexagonal pores of the TiO₂ samples. The rapid condensation of the precursor at the oil–water interface before its diffusion into the water channels maintains the integrity of the hexagonal water channels that are

responsible for the hexagonal pores of the materials. However, the gel-like mesophase appears to breakdown with reaction progress and the formation of the alcohol byproduct of TIP hydrolysis. We attribute the large pores formed in the particle interior to this gradual breakdown of the gel structure. In Figure 2, we also observe the side view of channels and the end view of the porous cross section. This is the consequence of templating in multiple crystalline domains that are randomly oriented. The result of templating in multiple randomly oriented domains has been described in our recent paper where the templated materials have been used in the catalytic process of CO oxidation.¹⁶

Figure 3 reveals the remarkable alignment effect of applying shear to the template system. Considerable improvement in directionality is achieved for titania samples synthesized in the sheared template compared to those obtained in the nonsheared template. These patterned channels are arranged parallel to each other, the result of aligning the domains of the crystalline domains as demonstrated by SANS.^{13,17} In such a relatively rigid system, once shear has been employed, the alignment of the ordered water channels persists for extended periods approaching a week, allowing the preparation of extended nanostructures.¹² The progression from mesochannels to macrochannels takes

(16) Sarkar, J.; John, V. T.; He, J. B.; Brooks, C.; Gandhi, D.; Nunes, A.; Ramanath, G.; Bose, A. *Chem. Mater.* **2008**, *20*, 5301.

(17) Liu, L. M.; Singh, M.; John, V. T.; Mcpherson, G. L.; He, J. B.; Agarwal, V.; Bose, A. *J. Am. Chem. Soc.* **2004**, *126*, 2276.

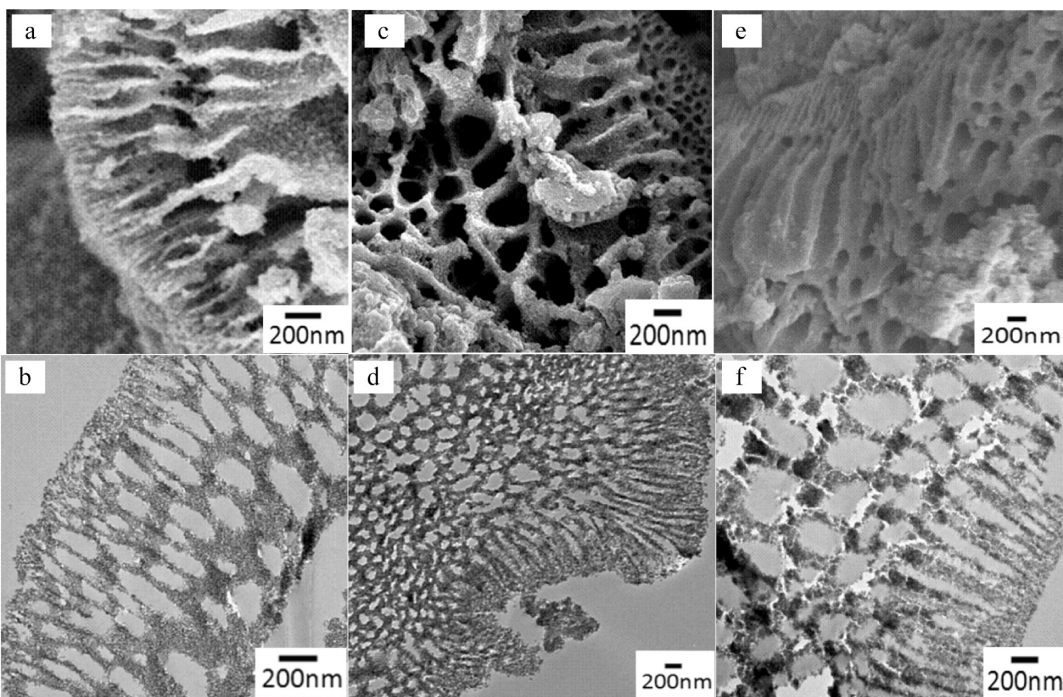


Figure 2. SEM (a, c, e) and cut-section TEM (b, d, f) images of nonsheared TiO_2 sample synthesized at different water content: (a, b) $W_0 = 70$, (c, d) $W_0 = 100$, and (e, f) $W_0 = 150$. The channels templated by the nonsheared gels run in different directions.

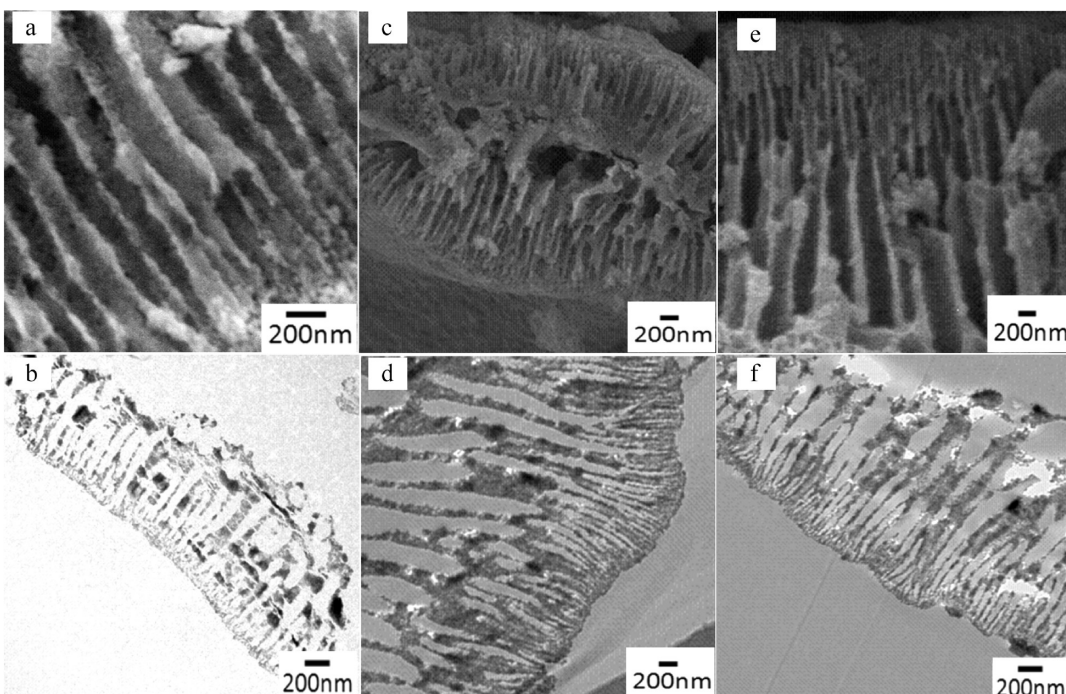


Figure 3. SEM (a, c, e) and cut-section TEM (b, d, f) images of sheared TiO_2 sample synthesized at different water content: (a, b) $W_0 = 70$, (c, d) $W_0 = 100$, and (e, f) $W_0 = 150$. The channels templated by the sheared gels run in the same direction.

place in a progressive manner, and the extension of the parallel arrayed channels throughout the material is clearly visualized from the side view SEM images (Figure 3a, c, e) and from the cut-section TEM images (Figure 3b, d, f). The process leads to the generation of open-ended large channels which may serve as ideal light transport routes to introduce more photoenergy into the interior of the titania. The largest channels with diameters 200–300 nm approach the wavelength of UV radiation.

Figure 4 illustrates further details of the nonsheared system (Figure 4a–c) and the sheared system (Figure 4d–f), focusing on

the large channels which may be more useful for photocatalytic applications. We observe a better definition of structure in the sheared system, which has relatively less debris in the channels (bottom set of micrographs). While there is a significant distribution in pore size, the average macropore size for the $W_0 = 70$ sample, as observed from the top view SEM images (Figure 4b, e) and the cut-section TEM images (Figure 4c, f), is approximately 100 nm. It is clear that the pore sizes are significantly larger than the pores in the original hexagonal template where the characteristic hexagonal d -spacing as observed by SANS is of the order

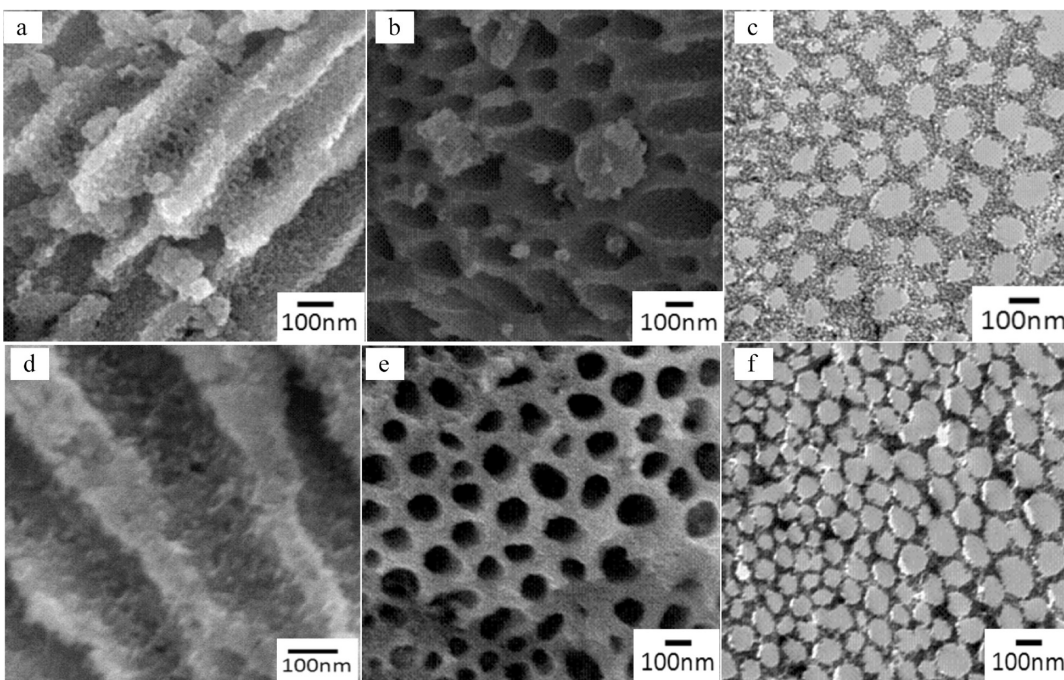


Figure 4. SEM and cut-section TEM images of TiO_2 samples synthesized at $W_0 = 70$: (a–c) nonsheared and (d–f) sheared. Secondary mesopores with diameter of approximately 5 nm branch out from the large macropores.

10–20 nm.¹¹ Again, we attribute the large pores to the breakdown of the soft template as TIP hydrolyzes and condenses into titania particles very quickly when contacted with moisture. The initial system simply contains TIP and the surfactants dissolved in isoctane, as a liquid micellar system. As the requisite amount of water is added, there is rapid reaction and spontaneous formation of the self-assembled crystalline mesophase created by water, isoctane, and the dual surfactant system. However, the two additional components here (TIP and the reaction product, propanol) affect the integrity of the gel pore structure and may lead to coalescence of the water channels as the reaction proceeds, leading to larger pore formation. Independent experiments with propanol added to the surfactant mesophase clearly demonstrate the breakdown of the gel. At the precursor concentrations used here, the propanol levels are low enough to not completely destroy the structure but to allow deterioration.

Figure 5 shows that the channel size of the TiO_2 samples can be controlled by adjusting the water content of the corresponding template mesophase. For example, the average channel diameter increases from 100 to 200 nm when the water content (W_0) is increased from 70 to 200 for sheared samples (same for non-sheared samples, images not shown here). However, the internal microstructure remains unaffected. We do note an interesting observation here. In surfactant gels of AOT/lecithin in water and isoctane, at water levels of $W_0 = 150$ and higher, the gel transits from a hexagonal structure to one containing multilamellar vesicles.¹¹ The continuation of the hexagonal templating morphology to the titania here is indicative of extremely fast transcription to solid ceramic when water is added to the system containing the TIP precursor. We assume that the initial structure transcribed to the solid is the hexagonal structure which persists even as water is added to levels exceeding the ability of the gels to sustain the hexagonal mesophase.

The microstructure of the sample was further analyzed using TEM and high-resolution TEM (HRTEM). Figure 6a reveals that the walls of the macroporous TiO_2 catalyst are composed of small interconnected TiO_2 nanoparticles with diameters

of 6–10 nm. Some interparticle pores about 5 nm can be observed in the walls, which correspond to the branched pores observed in Figure 4a and d SEM images. The electron diffraction pattern of the selected area (Figure 6a inset) exhibits several weak rings corresponding to the anatase crystals, indicating the polycrystalline structure of the titania walls. A representative HRTEM image of the sheared sample synthesized at $W_0 = 70$ is shown in Figure 6b, which reveals the presence of many crystallites with clear anatase lattice fringes, confirming that the walls consist of anatase nanocrystals. The XRD patterns show that the sheared and non-sheared TiO_2 samples synthesized at $W_0 = 70$ (the XRD patterns for $W_0 = 100, 150$, and 200 are the same those with $W_0 = 70$; data not shown) can be assigned to well-crystallized anatase TiO_2 (JCPDS 21-1272), as shown in Figure 6c. The broadening of the diffraction peaks have been caused by the small crystalline grain size (6–9 nm), which agrees with the TEM results in Figure 5b. The average crystalline size of TiO_2 nanoparticles can be calculated by applying the Scherrer equation to the anatase (101, $2\theta = 25.5^\circ$) diffraction peak, as listed in Table 1. It can be seen that the crystalline size increases with the W_0 values and the size is slightly larger for the sheared samples compared to the non-sheared samples. The diameters of the water channels are larger at higher water content (W_0), which can induce the precursor (titanium isopropoxide) of titania to hydrolyze quickly and completely at the water channel and organic phase interface, and also results in the larger crystalline size of the titania samples synthesized at higher W_0 values.

Figure 7 illustrates the nitrogen adsorption and desorption isotherms of the TiO_2 samples. All the curves demonstrate stepwise adsorption and desorption (type IV isotherms), with a hysteresis loop due to capillary condensation, indicating that the catalysts are mesoporous materials.¹⁸ The textural parameters obtained from the isotherms are listed in Table 1. The surface areas of the samples are comparable to that of the commercial

(18) Mariscal, R.; Lopez, G. M.; Fierro, J. L. G.; Sotelo, J. L.; Martos, C.; Grieken, V. *Langmuir* **2000**, *16*, 9460.

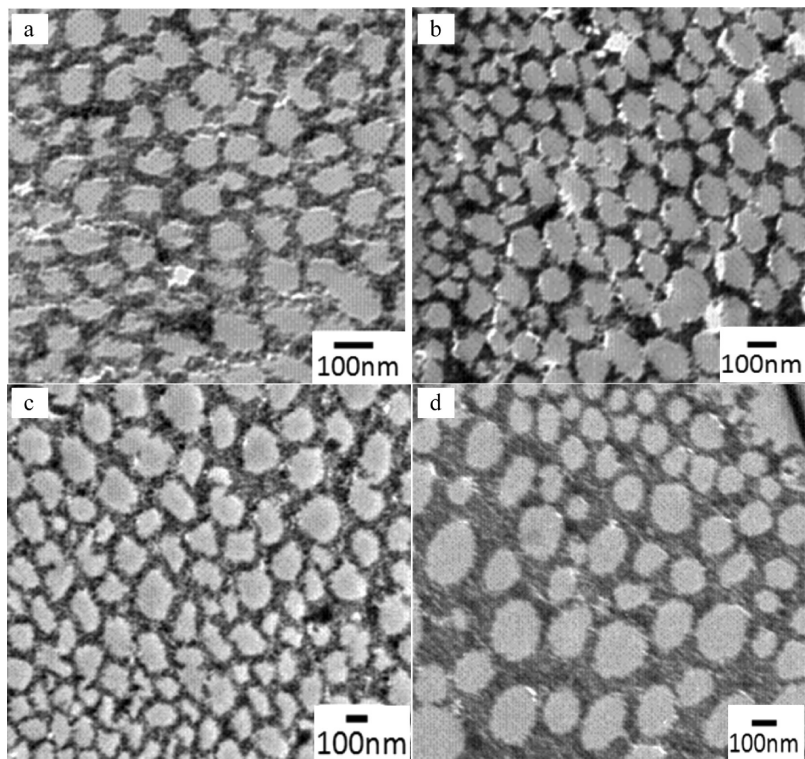


Figure 5. Cut-Section TEM images of sheared titania samples prepared at different water content: W_0 = (a) 70, (b) 100, (c) 150, and (d) 200.

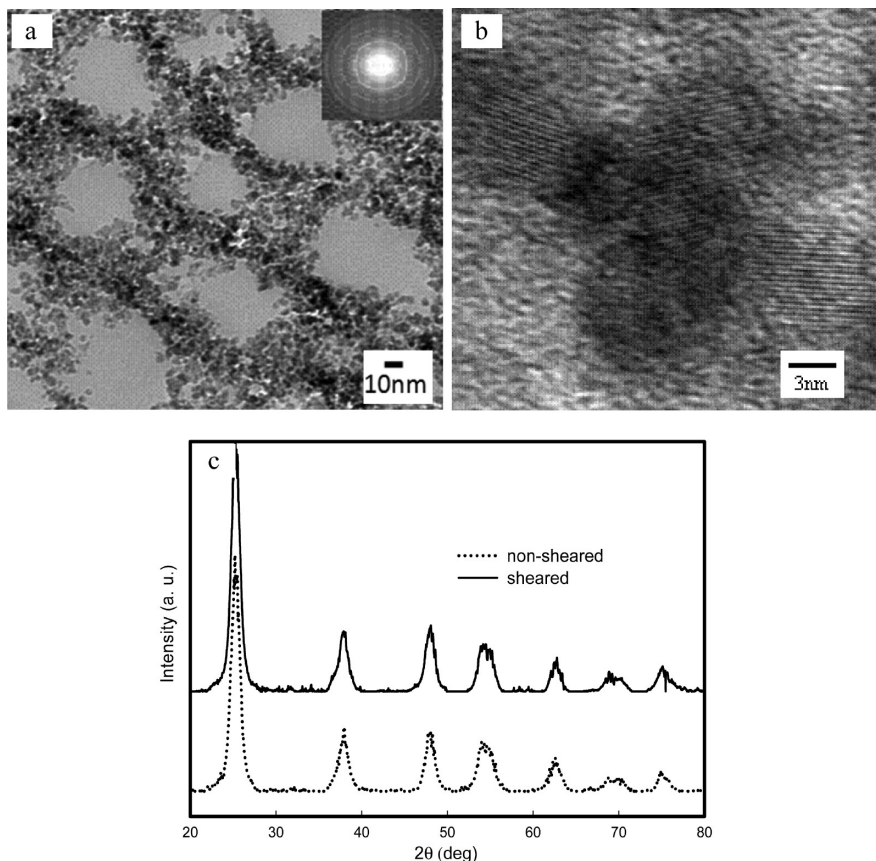


Figure 6. (a) Cut-section TEM and (b) HRTEM images of sheared TiO_2 samples synthesized at $W_0 = 70$. Walls of the macroporous TiO_2 catalyst are composed of small interconnected TiO_2 nanoparticles with diameters of 6–10 nm. X-ray diffraction patterns (c) show the anatase crystal structure of the samples.

Table 1. Physicochemical Properties of the Porous TiO₂ Samples from N₂ Sorption Analysis and XRD Results

water content	sheared samples				nonsheared samples			
	S _{BET} [m ² /g]	V [cm ³ /g] ^a	D _{BJH} [nm] ^b	crystalline size [nm]	S _{BET} [m ² /g]	V [cm ³ /g] ^a	D _{BJH} [nm] ^b	crystalline size [nm]
W ₀ = 70	41.5	0.12	9.3	7.1	76.1	0.22	8.3	6.6
W ₀ = 100	40.5	0.12	9.4	7.4	64.3	0.22	8.9	6.8
W ₀ = 150	47.9	0.14	9.4	7.8	25.7	0.10	10.9	7.8
W ₀ = 200	31.3	0.12	12.3	8.9	25.7	0.08	13.8	8.0

^aTotal pore volume, obtained from the volume of N₂ adsorption at P/P₀ = 0.995. ^bAverage pore diameter, estimated using the desorption branch of the isotherm.

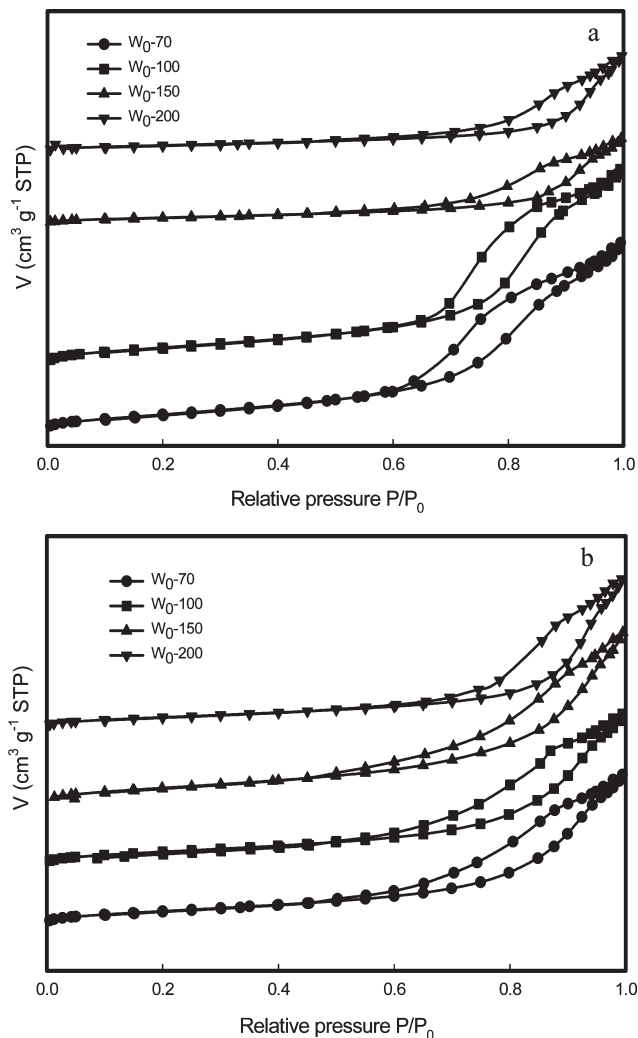


Figure 7. Nitrogen adsorption–desorption isotherms of TiO₂ samples: (a) nonsheared and (b) sheared.

Degussa P-25. The products synthesized at lower W₀ values always have larger surface areas due to their smaller channels.

The photocatalytic activity of the samples was examined by measuring the photodegradation of Rhodamine B in an aqueous suspension of titania. To account for the possible decrease in dye concentration due to heat generated from irradiation, a control experiment without any catalyst in the solution was carried out. There was almost no decrease in Rhodamine B concentration after 100 min irradiation in the absence of TiO₂. All titania samples exhibit good photocatalytic activity with degradation of approximately 50% of the dye upon 30 min irradiation. When the samples are irradiated for 80 min, the degradation percentage of Rhodamine B with catalyst is approximately 90%, as shown in Figure 8. The decay in concentration follows pseudo-first-order

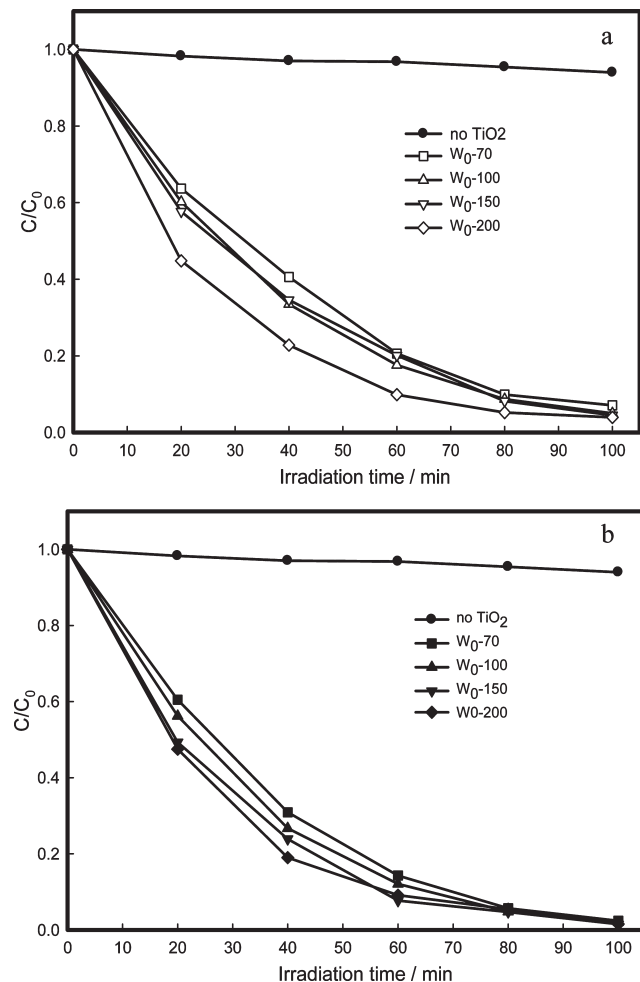


Figure 8. Photocatalytic degradation of Rhodamine B monitored as the normalized concentration change versus irradiation time in the presence of as-synthesized titania samples; C and C₀ represent the concentrations of the dye at t time and the initial concentration: (a) nonsheared and (b) sheared.

kinetics consistent with previous reported results on titania photocatalysis of Rhodamine B.^{4,19} The rate constants are calculated to be 0.0378, 0.0396, 0.0417, and 0.041 min⁻¹ for the sheared titania samples synthesized at water contents of 70, 100, 150, and 200, while those for nonsheared samples exhibit slightly lower values of 0.0278, 0.0306, 0.0313, and 0.033 min⁻¹, respectively. The results indicate that patterned organization of the macropores has an enhancement effect on the photoactivity of the catalyst (the photocatalytic activities increase by 36.0%, 32.7%, 33.2%, and 23.3%, respectively, for sheared TiO₂ samples compared to those of the nonsheared TiO₂ samples). The higher

(19) Zhang, D. Y.; Yang, D.; Zhang, H. J.; Lu, C. H.; Qi, L. M. *Chem. Mater.* 2006, 18, 3477.

photocatalytic performance of the sheared sample may be interpreted in terms of the interconnected porous walls as well as the highly patterned channel arrays. Additionally, the titania materials prepared at higher W_0 values show higher photocatalytic activities although their surface areas are always lower. We ascribe this to the fact that the average channel distribution increases from 100 to 200 nm with the increase of W_0 . The larger channels may increase light penetration and enhance the photoabsorption efficiency. There could be other secondary effects including the fact that there appears to be more “debris” in the channels of the samples prepared at lower water contents, which may further decrease light access to the particle interior.

Unfortunately, in the system studied here, the activities of the porous anatase TiO_2 samples are lower than that of P-25 (0.10 min^{-1}). The reason is not clear because the surface areas of our samples ($25\text{--}70 \text{ m}^2/\text{g}$) are comparable to that of P-25 ($53 \text{ m}^2/\text{g}$). The relatively higher activity of P-25 is due to its mixed crystal phase of anatase and rutile titania which is favorable to the separation of photogenerated electrons and holes.²¹ We note that Yu et al. reported that macro/mesoporous anatase TiO_2 showed higher photocatalytic activity ($3.78 \times 10^{-3}\text{--}6.13 \times 10^{-3} \text{ min}^{-1}$) than P-25 ($3.01 \times 10^{-3} \text{ min}^{-1}$) for the degradation of acetone in air.²⁰ This was explained by the high specific surface areas ($104\text{--}206 \text{ m}^2/\text{g}$) and hierarchical macro/mesoporous structures ($2\text{--}4 \mu\text{m}$ macrochannels) which allowed significant light entry to the particle interior. The aspects of surface area and phase composition correlated to photocatalytic efficiencies need further study with a model reaction over a variety of well-characterized materials before consistent trends are realized and explained.

The enhancement of photoactivity of a catalyst can be realized by increasing the photoabsorption energy of the material and the collision efficiency between the reactant molecules and the photoactive sites. In the present study, the open-ended highly patterned channels in the sheared samples can act as ideal light transport routes and permit light to pass through the porous materials, introducing incident photo flux into the interior of the catalyst.^{20,22} Therefore, an increase in the photoabsorption efficiency can be achieved by the adsorption, reflection, and scattering of the deep penetration light introduced into the channels. Also, more photoactive sites on the channel surface are activated, and more positive holes and electrons are generated, which is of central importance for the degradation reaction. It has been reported that a 320 nm wavelength light is diminished to 10% of its original intensity after penetrating a distance of $8.5 \mu\text{m}$ on condensed titania.²³ For our sheared samples shown in Figure 3, the length of the channels is only several hundred nanometers and they are

arranged parallel to each other. It is reasonable that the light intensity not be heavily extinguished after penetrating the material. Furthermore, the branched pores embedded in the walls act as small passages linking the patterned channels, allowing the reactant molecules to diffuse and transport within the porous framework. This facilitates the collision of the reactant molecules with more photoactive sites and hence increases the reaction rate. The transport and diffusion rates of small molecules in media featuring mesopores ($>10 \text{ nm}$) and macropores ($>50 \text{ nm}$) are comparable to those in an open nonporous medium.²⁴ Here, we can speculate that reactant molecules can freely move in and out of the porous sheared titania materials, as the diffusion resistance of molecules can be easily overcome in $100\text{--}200 \text{ nm}$ channels.

Conclusion

In summary, porous TiO_2 materials with an aligned channel structure were synthesized using a dual surfactant mesophase. These materials were obtained by applying shear to the soft template, thereby aligning hexagonal crystalline domains of the template. The structure of the template deteriorates with reaction process, but the deterioration becomes captured in the ceramic where narrow pore structures meld into larger ones, leading to a system of increasing channel diameters. The patterned channels arranged parallel to each other could act as an ideal light transfer pathway for introducing UV light into the interior of the catalyst. This would enhance the photoabsorption efficiency as well as the efficiency of the photogenerated electrons/holes in the sheared titania samples, leading to higher photocatalytic activity for degradation of Rhodamine B compared to the nonsheared samples. Additionally, reactant molecules can transport and diffuse through the channels and branched pores, which are partly responsible for its higher photocatalytic activity. These porous materials with aligned channels, high photoabsorption efficiency, and progressively increasing channel size distribution may be promising as advanced catalytic supports and as novel optic or photoelectric materials. Due to having a unique structure with $10\text{--}20 \text{ nm}$ pores at the surface and $100\text{--}200 \text{ nm}$ channels in the interior, such porous materials may have applications in the synthesis of asymmetric ceramic membranes.²² Additionally, due to the biocompatibility of TiO_2 , such materials may have applications in the design of drug delivery systems allowing transport of biomacromolecules through the macrochannels of the materials.

Acknowledgment. We are grateful for financial support from the National Science Foundation (Grant 0438463), from NASA (Grant NAG-1-02070), and from the Advanced Materials Research Institute at the University of New Orleans. Financial support from the China Scholarship Council for an exchange visitor scholarship to X.L. is gratefully acknowledged.

(24) Rolison, D. R. *Science* **2003**, 299, 1698.

(20) Yu, J. G.; Su, Y. R.; Cheng, B. *Adv. Funct. Mater.* **2007**, 17, 1984.

(21) (a) Xu, H.; Jia, F. I.; Ai, Z. H.; Zhang, L. Z. *Cryst Growth Des.* **2007**, 7, 1216.
(b) Yu, J. G.; Zhang, L. J.; Cheng, B.; Su, Y. R. *J. Phys. Chem. C* **2007**, 111, 10582.

(22) Choi, H.; Sofranko, A. C.; Dionysiou, D. D. *Adv. Funct. Mater.* **2006**, 16, 1067.

(23) Hagfeldt, A.; Gratzel, M. *Chem. Rev.* **1995**, 95, 49.